Chromatin organization by an interplay of loop extrusion and compartmental segregation

Johannes Nuebler[a], Geoffrey Fudenberg[b], Maxim Imakaev[a], Nezar Abdennur[a], and Leonid A. Mirny[a,1]

[a]Department of Physics, Institute for Medical Engineering and Science, Massachusetts Institute of Technology, Cambridge, MA 02139; and [b]Gladstone Institutes of Data Science and Biotechnology, San Francisco, CA 94158

Edited by Robert H. Singer, Albert Einstein College of Medicine, Bronx, NY, and approved June 4, 2018 (received for review October 10, 2017)

Mammalian chromatin is spatially organized at many scales showing two prominent features in interphase: (*i*) alternating regions (1–10 Mb) of active and inactive chromatin that spatially segregate into different compartments, and (*ii*) domains (<1 Mb), that is, regions that preferentially interact internally [topologically associating domains (TADs)] and are central to gene regulation. There is growing evidence that TADs are formed by active extrusion of chromatin loops by cohesin, whereas compartmentalization is established according to local chromatin states. Here, we use polymer simulations to examine how loop extrusion and compartmental segregation work collectively and potentially interfere in shaping global chromosome organization. A model with differential attraction between euchromatin and heterochromatin leads to phase separation and reproduces compartmentalization as observed in Hi-C. Loop extrusion, essential for TAD formation, in turn, interferes with compartmentalization. Our integrated model faithfully reproduces Hi-C data from puzzling experimental observations where altering loop extrusion also led to changes in compartmentalization. Specifically, depletion of chromatin-associated cohesin reduced TADs and revealed finer compartments, while increased processivity of cohesin strengthened large TADs and reduced compartmentalization; and depletion of the TAD boundary protein CTCF weakened TADs while leaving compartments unaffected. We reveal that these experimental perturbations are special cases of a general polymer phenomenon of active mixing by loop extrusion. Our results suggest that chromatin organization on the megabase scale emerges from competition of nonequilibrium active loop extrusion and epigenetically defined compartment structure.

chromatin | genome architecture | Hi-C | polymer physics | active matter

Eukaryotic chromatin, that is, DNA together with associated proteins, is far from being simply a randomly arranged polymer in the cell nucleus. Investigations into its spatial organization by chromosome conformation capture (1) and its descendent Hi-C (2) have revealed two salient features in higher eukaryotes. First, at the supermegabase scale, chromatin spatially segregates into different compartments (2). The Hi-C signature of segregation is a plaid, or checkerboard, pattern (Fig. 1*A*), which indicates that chromatin of a given type preferentially interacts with other loci of the same type (3, 4). Spatial segregation is further supported by imaging of individual loci (5, 6) and whole compartmental segments (7). The second striking feature of 3D organization are topologically associating domains (TADs) (8, 9). Their Hi-C signature are squares along the diagonal, indicating local regions of increased contact frequency, typically on the submegabase scale.

Several lines of evidence indicate that compartments and TADs are formed by distinct mechanisms and are not a hierarchy of the same phenomenon on different scales. First, TADs have no checkerboard pattern in Hi-C (Fig. 1 and ref. 8). Second, the alternating compartment structure correlates with gene density, gene expression, and activating epigenetic marks, which are all enriched in compartments of type A (2), while no such classification has been reported for TADs. Rather, TAD boundaries, not their interior, are associated with architectural proteins, in particular CTCF (8, 9). Also, TADs are less cell type-specific than compartments (8, 9). Furthermore, TADs can exist without compartments and vice versa (10). Finally, recent experiments directly showed that TADs compete with compartments: Removal or depletion of chromatin-associated cohesin (11–14), which is required for TADs, not only made TADs disappear but also increased compartmentalization (11, 12, 14), sharpened compartment transitions (13), and fragmented compartments into shorter intervals (11) (see Fig. 1*A* for a cartoon and Fig. 2*A* for an example). Strikingly, these finer compartments match epigenetic marks of activity better than the more coarse wild-type (WT) compartments (11), suggesting that the loss of cohesin activity reveals the underlying innate compartment structure that is obscured in the WT. The opposite effect was achieved by increasing the residence time and the amount of cohesins on DNA: TADs were extended and compartmentalization weakened (12, 14) (see Fig. 2*C* for an example). These observations raise the question of how cohesin, crucial for forming TADs, could mechanistically alter compartmentalization.

TADs are believed to be formed by active extrusion of chromatin loops (15, 16), which has appeared multiple times in the literature as a mechanism for chromosome organization (17–20): Loop extrusion factors (LEFs) attach to the chromatin fiber and start progressively enlarging a DNA loop until they either fall off, bump into each other, or bump into extrusion barriers, which define the TAD boundaries (Fig. 1*B*). Active loop extrusion explains many features of TADs (15, 16): (*i*) TADs have no

Significance

Human DNA is 2 m long and is folded into a 10-μm-sized cellular nucleus. Experiments have revealed two major features of genome organization: Segregation of alternating active and inactive regions into compartments, and formation of compacted local domains. These were hypothesized to be formed by different mechanisms: Compartments can be formed by microphase separation and domains by active, motor-driven, loop extrusion. Here, we integrate these mechanisms into a polymer model and show that their interplay coherently explains diverse experimental data for wild-type and mutant cells. Our results provide a framework for the interpretation of chromosome organization in cellular phenotypes and highlight that chromatin is a complex, active matter shaped by an interplay of phase segregation and loop extrusion.

Author contributions: J.N. and L.A.M. designed research; J.N., G.F., M.I., and N.A. performed research; and J.N., G.F., M.I., N.A., and L.A.M. wrote the paper.

The authors declare no conflict of interest.

This article is a PNAS Direct Submission.

[1]To whom correspondence should be addressed. Email: leonid@mit.edu.

This article contains supporting information online at www.pnas.org/lookup/suppl/doi:10.1073/pnas.1717730115/-/DCSupplemental.

Published online July 2, 2018.

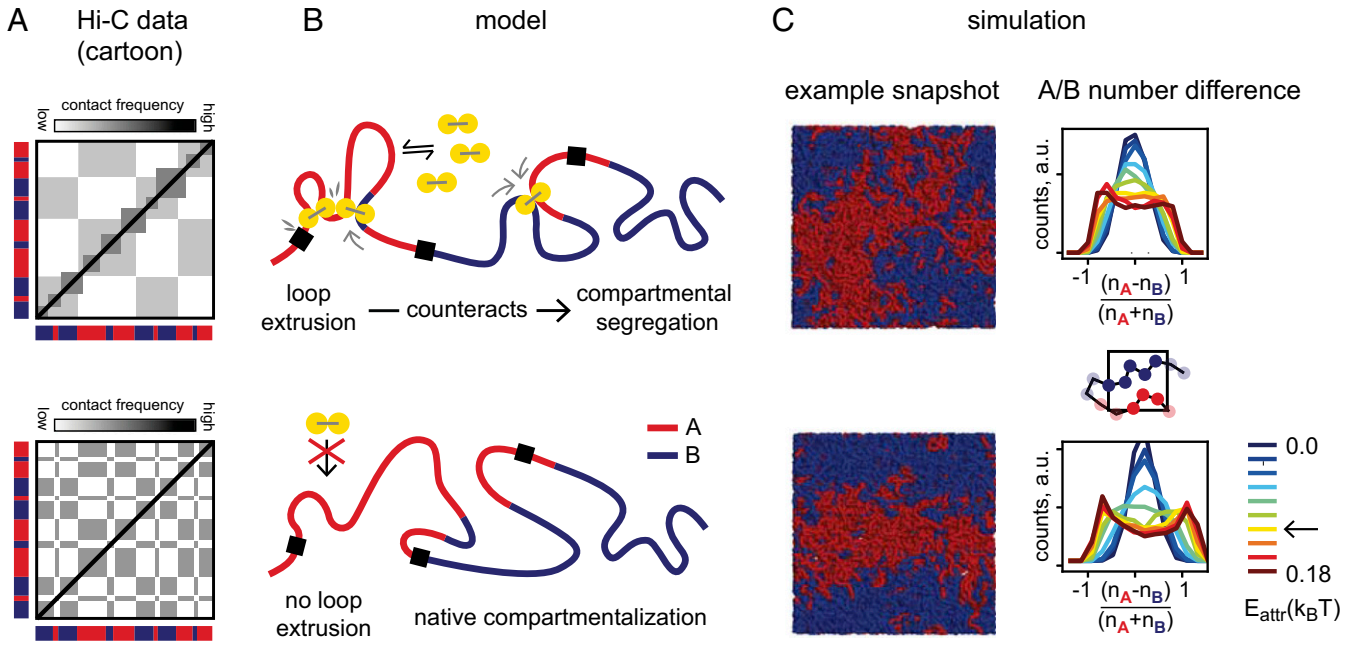

Fig. 1. Model of loop extrusion competing with compartmental phase separation. (*A*) Cartoon of typical Hi-C signatures of interphase chromatin organization: Topologically associating domains (TADs) are squares of increased contact frequency along the diagonal, while compartmentalization is a checkerboard pattern indicating spatial segregation. Upon removal of the cohesin loader Nipbl, Schwarzer et al. (11) observed that TADs disappear and a fine-scale compartmentalization emerges (indicated in red/blue; see Fig. 2*A* for a data example). (*B*) Sketch of our mechanistic model: Loop extrusion factors (LEFs) (yellow) counteract segregation of A (red)- and B (blue)-type chromatin. (*C*) Simulations. (*Left*) Example conformations from polymer simulations showing phase separation of A and B regions (here in periodic boundary conditions). (*Right*) The emergence of an A-rich and a B-rich phase in our simulations is quantified by the normalized number difference of A and B particles in small boxes, which becomes bimodal as the compartmental interaction E_{attr} is increased (colors from blue to red; the arrow indicates the value used throughout the text; $E_{attr} = 0.12\ k_BT$).

checkerboard signature in Hi-C; (*ii*) removal of a TAD boundary leads to the fusion of two TADs into a larger one; (*iii*) the sequence motifs at TAD boundaries have a specific, convergent, orientation as they oppose loop extrusion unidirectionally; and (*iv*) TAD corner peaks arise from loop extruders bringing TAD boundaries into spatial proximity.

The proposed molecular candidates for LEFs are structural maintenance of chromosome (SMC) protein complexes (21, 22), in particular cohesin during interphase (23). Cohesin topologically entraps DNA (24), can slide along DNA and over small DNA-bound proteins and nucleosomes (25, 26), and is enriched at TAD boundaries (9) and corner peaks (27). It was shown recently in vitro that a closely related SMC, yeast condensin, has ATP-dependent motor activity (28), and growing loops were directly visualized (29). Furthermore, bacterial condensins processively juxtapose the bacterial chromosome in vivo (30). Cohesin is loaded onto eukaryotic DNA, assisted by Nipbl (31), while WAPL limits its residence time (32, 33). Central to the formation of TAD boundaries is the protein CTCF: It is enriched and conserved at TAD boundaries (8, 9), and disruption of CTCF binding sites alters TAD structure (15, 34–37).

Compartmental segregation of active and inactive chromatin is evident from microscopy (7, 38) and manifests as checkerboard pattern in Hi-C maps (2), but cannot be explained by loop extrusion. While the exact segregation mechanism and its molecular players have yet to be identified, a natural class of models are block copolymers (39, 40). A block copolymer consists of alternating blocks of monomers of different types (e.g., A blocks and B blocks) that have different affinities for each other. In such polymer systems, different blocks can form separate spatial compartments (41–43). These models are further motivated by the observed partitioning of chromatin into a small number of types based on histone modifications (27, 44), which may in turn entail different affinities for each other, including via histone tails (45), and recruitment of HP1 or other proteins (46, 47). An integrated model that includes both compartmentalization and loop extrusion is largely missing. While Rao et al. (13) illustrate how the pattern of compartments and TADs change in simulations upon loss of loop extrusion in a single 2-Mb locus, a systematic characterization and a physical examination of how the nonequilibrium active loop extrusion process affects global compartmentalization are essential for understanding large-scale chromosome organization.

Here, we address the question of how cohesin-mediated loop extrusion can interfere with compartmentalization of heterochromatin and euchromatin. Using polymer simulations, we examine chromatin compartmentalization by phase separation and show that active mixing by loop extrusion locally counteracts compartmentalization. Our model agrees with several recent experiments where reduction or increase in loop-extrusion activity had different effects not only on TADs but also on compartments. Our model also makes specific predictions for future experiments and explains how the interplay of loop extrusion and compartmental segregation shapes chromosome organization in interphase.

Results

Polymer Model of Loop Extrusion. To investigate the interplay of loop extrusion with compartmentalization, we simulate the chromatin fiber as a polymer subject to loop extrusion and compartmental segregation (Fig. 1). LEFs can attach to the chromatin polymer at random positions and extrude loops bidirectionally until they either fall off, bump into each other, or encounter an extrusion barrier. When blocked on one side, they continue extruding unidirectionally. LEFs are characterized by three parameters: the average residence time τ, the single-sided extrusion velocity v, and the average separation d (48). The first two define the processivity as $\lambda = 2\tau v$, which is the average size of a loop

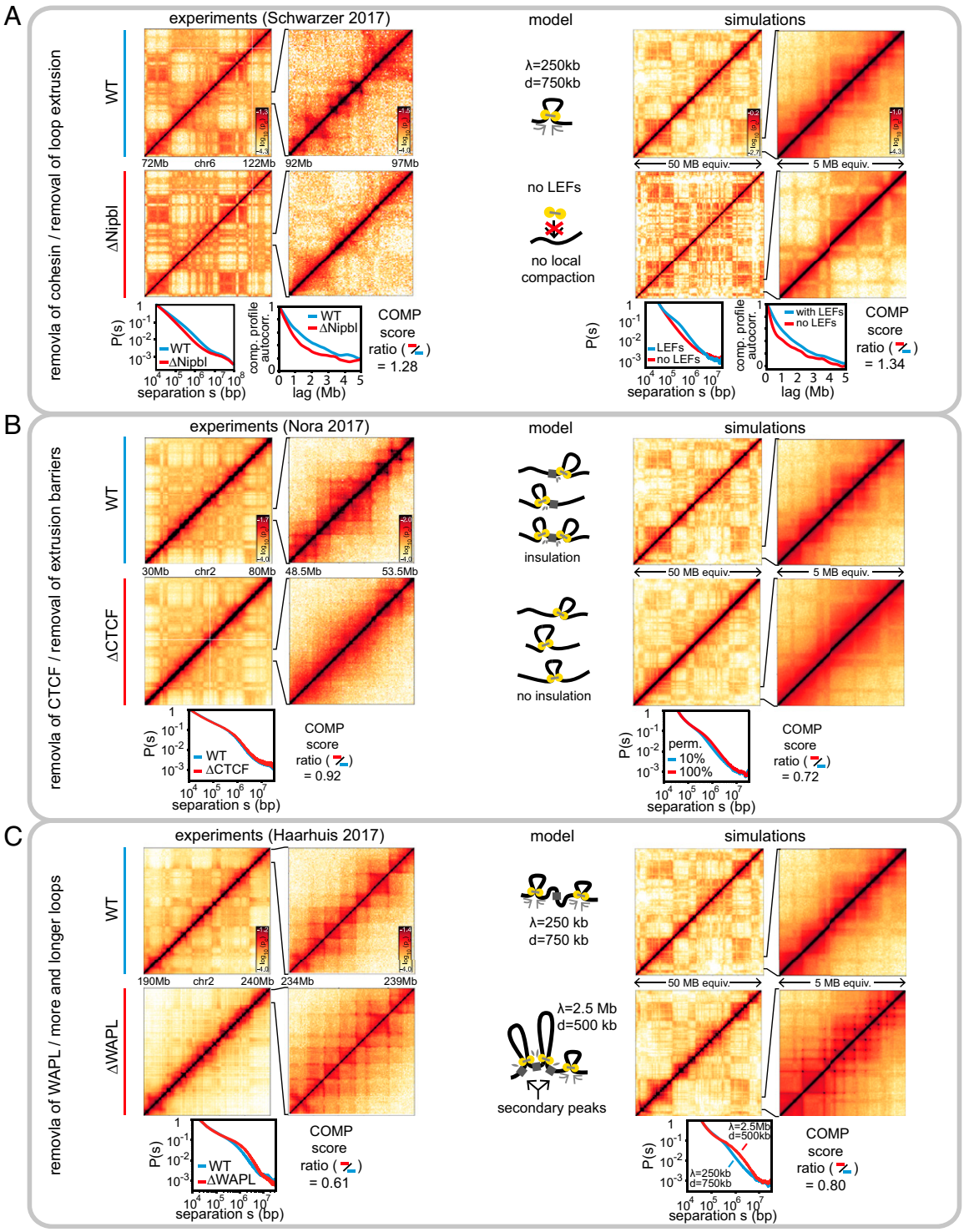

Fig. 2. Experiments and simulations show the interplay of loop extrusion and compartmentalization. (*A*) Removal of chromatin-associated cohesin (by knockout of the cohesin loader Nipbl)/removal of loop extrusion. (*Left*) Cohesin removal leads to stronger and fragmented compartmentalization and loss of TADs. Data from ref. 11. (*Right*) The same is observed in simulated Hi-C maps upon removal of loop extrusion. The loss of loop extrusion leads the loss of a characteristic hump in $P(s)$, the contact probability as a function of genomic separation. The fragmentation is apparent in compartment profiles as the faster decay of their autocorrelation. The degree of compartmentalization (COMP score) is reduced by a similar factor upon removal of Nipbl/loop extrusion in experiments/simulation. (*B*) Removal of CTCF/removal of extrusion barriers. (*Left*) CTCF depletion strongly suppresses TADs but leaves compartmentalization almost unaffected. Data from ref. 37. (*Right*) The same is observed in simulations when loop extrusion barriers are removed (barrier permeability increased from 10 to 100%). LEF processivity λ and average separation d are as in *A*. The decay of the contact probability with genomic distance barely changes both in experiments and simulations. (*C*) Increased activity of cohesin (by knockout of the cohesin unloader WAPL)/more and longer loops. (*Left*) Removal of WAPL reduces compartmentalization and strengthens TADs, in particular secondary corner peaks. Data from ref. 12. (*Right*) The same is observed in simulations with a 10-fold increase in LEF processivity and a 1.5-fold increase in LEF density. The secondary corner peaks arise when the chromatin between barriers is fully extruded, forming contacts between several consecutive barriers (*Lower* cartoon). The characteristic hump in contact probability scaling extends to significantly larger distances, reflecting larger loops (14).

extruded by an unobstructed LEF. Simulation parameters are given in Table 1. For WT, we use $\lambda/d = 1/3$; cells thus operate in the dilute regime ($\lambda/d < 1$), where LEFs rarely bump into each other. CTCF-enriched boundaries of TADs are modeled by barriers that block extrusion of LEFs with probability 90% in WT (16). Having a finite permeability is consistent with the turnover time of CTCF being considerably shorter than that of cohesin [≈1–2 min (49, 50) vs. >5–30 min (12, 50–53)], although the exact value of the permeability may vary across the genome and may depend on the number and occupancy of CTCF sites, cofactors, and details of interactions between CTCF and cohesin. Values of these and other parameters are chosen to reproduce TAD patterns observed in Hi-C data and are systematically varied to examine their effects on chromatin organization. Positions of the TAD boundaries are randomly generated based on the above characteristics. They are not intended to reproduce specific genomic regions, since our goal is to demonstrate that a single model can reproduce genome-wide quantities from three different phenotypes (removal of cohesin, CTCF, and WAPL) observed in different organisms (mouse and human). In our simulations, loop extrusion is effective in both compartment types, consistent with the presence of TADs in experimental Hi-C in both A and B regions. Unless otherwise mentioned, we allow for some passing of two parts of the chromatin fiber through each other by imposing a finite repulsive core on the monomer interaction potential (*SI Appendix*, Fig. S1). This represents the effect of topoisomerase II and is discussed further below.

Compartmental Segregation by Phase Separation. Compartment organization is modeled by a block copolymer composed of A and B blocks that have the same local properties (monomer size and fiber flexibility) but interact differently. Positions of A and B blocks are randomly generated with sizes of blocks chosen to yield an autocorrelation length of the compartment profile inferred from experimental Hi-C data (*SI Appendix*). The spatial segregation of A- and B-type chromatin is induced by a weak B–B attraction, which we refer to as compartmental interaction. It is parametrized by E_{attr}, the minimum value of the monomer interaction (*SI Appendix*, Fig. S1*A*), but can also be modeled differently (*SI Appendix*, Fig. S1*E*). This is sufficient to induce compartmental segregation in the absence of anchoring to the lamina (54). We choose the interaction parameter $E_{attr} = 0.12\ k_BT$ to achieve a similar degree of compartmentalization (see below) in experiments and simulations. We point out that this attraction is far too weak to turn B regions into a collapsed polymer state: The densities in the A-rich and B-rich phase differ by only about 10% (*SI Appendix*, Fig. S1*D*). Taken together, within our model, heterochromatin is phase separated from euchromatin, but not collapsed (*Discussion*).

To quantify the degree of phase separation, we examine the local densities of A and B monomers in small boxes and compute the normalized difference of A and B particles per box: $(n_A - n_B)/(n_A + n_B)$ (histograms in Fig. 1*C*). As we increase E_{attr}, the histograms become bimodal, which demonstrates the emergence of an A-rich and a B-rich phase. As an order parameter, we compute the mean absolute value of the normalized number difference, $N = <|(n_A - n_B)/(n_A + n_B)|>$ (*SI Appendix*, Fig. S1*C*), which shows the microphase separation characteristic of block copolymers. The phase separation is reduced by the presence of loop extrusion, which we will explore in detail throughout the paper.

Table 1. Simulation parameters for WT and mutant cells

Condition	Processivity λ	Separation d, kb	Permeability, %
WT	250 kb	750	10
ΔNipbl	—	—	—
ΔCTCF	250 kb	750	100
ΔWAPL	2.5 Mb	500	10

Loop extrusion factor (LEF) processivity λ, LEF separation d, and permeability of extrusion barriers for simulation of WT cells and removals (Δ) of the cohesin loading factor Nipbl, the TAD boundary protein CTCF, and the cohesin unloading factor WAPL. In ΔNipbl, no LEFs are present. Other simulation parameters are given in *SI Appendix*.

The degree of compartmentalization can also be computed from contact frequencies for both simulated and experimental Hi-C maps as the normalized contact frequency difference between same-type contacts, AA and BB, and different-type contacts AB, namely COMP = (AA + BB − AB)/(AA + BB + AB). We point out that our compartmentalization score measures the checkerboard contrast of a contact map and is by construction independent of the contact probability scaling $P(s)$ (*SI Appendix*). For simulated data, the compartmental identities of all loci are known, while for experimental data they need to be inferred from the Hi-C maps. To do so, we compute compartment profiles from eigenvector decomposition of the Hi-C maps (2, 3) and assign compartmental segments of type A/B to intervals with positive/negative compartment profile. Note that a locus of a given type may not be able colocalize with other loci of the same type. Compartmental segments assigned from Hi-C maps may thus differ from the underlying A/B types of the loci (*SI Appendix*).

Loop Extrusion Overrides Compartmentalization on Small Scales. Our central finding is that the active process of loop extrusion counteracts compartmental segregation. We determine this from three different experimental datasets where the loop extrusion machinery was altered in different ways, and from our corresponding polymer simulations. First, we test whether our integrated model can explain the effects of depleting chromatin-associated cohesin (11), namely, disappearance of TADs and simultaneous changes in compartmentalization such as (*i*) compartmental segments that span several megabases to several tens of megabases appear more crisp in Hi-C, and (*ii*) they become fragmented into smaller segments (Fig. 2*A*, *Left*). Strikingly, loss of loop extrusion in our model reproduces both phenomena (Fig. 2*A*, *Right*): While TADs disappear, compartmentalization, in particular of small segments, is enhanced, leading to fragmentation of large compartmental segments. Our simulations thus show that loop extrusion suppresses the inherent compartmentalization by counteracting segregation of small segments, which emerges when loop extrusion is removed.

We quantify changes in simulated chromatin upon loss of loop extrusion and compare them to changes in experimental data from ref. 11 in three ways (Fig. 2*A*, *Lower* graphs). (*i*) The removal of loop extrusion is detected by changes in the contact frequency as a function of genomic distance, $P(s)$: With loop extrusion, the $P(s)$ curve shows a characteristic hump on the length scale of TADs. This hump disappears upon removal of loop extrusion both in experiments and simulations. (*ii*) The strengthening of short compartmental segments ("fragmentation" of compartments) upon loss of loop extrusion is quantified by the steeper decay of the autocorrelation of the compartment profile. This steepening is evident in simulations and experiments alike. (*iii*) The greater contrast in Hi-C maps upon removal of loop extrusion is measured by changes in the degree of compartmentalization (see above and *SI Appendix*). Its increase in simulations is slightly stronger than in experiments, which could indicate that some compartment mixing remains present in experiments, either by residual cohesin (*SI Appendix*, Fig. S2) or some other processes in the nucleus not considered here (note in *SI Appendix*).

Most importantly, our simulations show that loop extrusion suppresses small compartmental segments more than large ones.

We study this in detail with simulations of uniformly sized compartmental segments (Fig. 3). For small segment lengths (<320 kb, i.e., <128 monomers), we observe little compartmental segregation even in the absence of loop extrusion, while larger segments show a clear phase separation, with transition at about 500 kb. The phenomenon of a length-dependent transition is known from the physics of block copolymers: It occurs when the product of segment length and compartmental interaction parameter exceeds a critical value (40). Here, we find that adding loop extrusion shifts this phase transition to larger segments of ≈1 Mb (Fig. 3*D*, Middle). For example, 800-kb segments are segregated in the absence of loop extrusion but get largely mixed in its presence (Fig. 3 *A*–*C*, second panels from *Left*). For even larger segment lengths, loop extrusion has diminishing effects. For example, for 2-MB segments segregation is only slightly reduced by loop extrusion (Fig. 3 *A*–*C*, third panels from *Left*). We attribute this size-dependent impact of loop extrusion on compartmentalization to two effects: (*i*) Segregation of shorter compartmental segments are weaker to begin with, and can be easily perturbed by active mixing due to loop extrusion; (*ii*) LEFs cannot mix segments that considerably exceed their average processivity (here, $\lambda = 250$ kb). To summarize, the impact of loop extrusion on segregation, computed as the ratio of compartmentalization measures without and with LEFs (Fig. 3*D*, *Right*), is most pronounced for compartments of 500 kb to 2 Mb since very small compartmental segments (<320 kb) do not segregate even without loop extrusion, while large compartments (>2 Mb) remain largely unaffected.

These results are in very good agreement with recent cohesin depletion experiments that reveal finer-scale compartmentalization: Small compartmental segments are suppressed by loop extrusion in WT cells and emerge in the mutant without loop extrusion; large compartments are present in both cases but may be diminished by loop extrusion. Our simulations suggest that the emergent fine structure is the intrinsic compartmentalization that is overridden in WT cells by loop extrusion by cohesin. This is in line with the observation that epigenetic marks correlate better with finer emergent than with the coarser WT compartmentalization (11). Taken together, our results suggest that loop extrusion suppresses the inherent compartmental segregation on the length scale of several cohesin processivities and leaves only larger-scale compartmentalization visible. When loop extrusion is removed by depletion of chromatin-associated cohesin, the intrinsic compartmental segregation emerges.

Removing Loop Extrusion Barriers Suppresses TADs but Not Compartments. Next, we asked whether our model of loop extrusion and compartmental segregation is compatible with depletion experiments of the TAD boundary element CTCF (37). Namely, CTCF depletion leads to a loss of TAD boundaries while having little effect on compartmentalization (Fig. 2*B*, *Left*). We simulated CTCF depletion by removing extrusion barriers, which led to a 1.2-fold increase in loop size (from 173 to 216 kb). In agreement with experiments, we observe a loss of TADs, while compartmentalization is mostly unaffected (Fig. 2*B*, *Right*; see *SI Appendix*, Fig. S3 for a parameter sweep). Unlike in cohesin depletion, no fine compartmentalization emerges. The distinction from cohesin depletion arises because upon CTCF removal loop extrusion is still present, but not restricted to specific domains.

Although TADs are diminished upon both CTCF removal and cohesin loss, these two perturbations have vastly different effects on chromatin organization. The lack of changes in $P(s)$ curves upon CTCF removal suggest that local chromatin compaction by loop extrusion is unaffected, as evident from the hump for $s < 1$ Mb in the $P(s)$ curve. Our simulations reproduce this phenomenon:

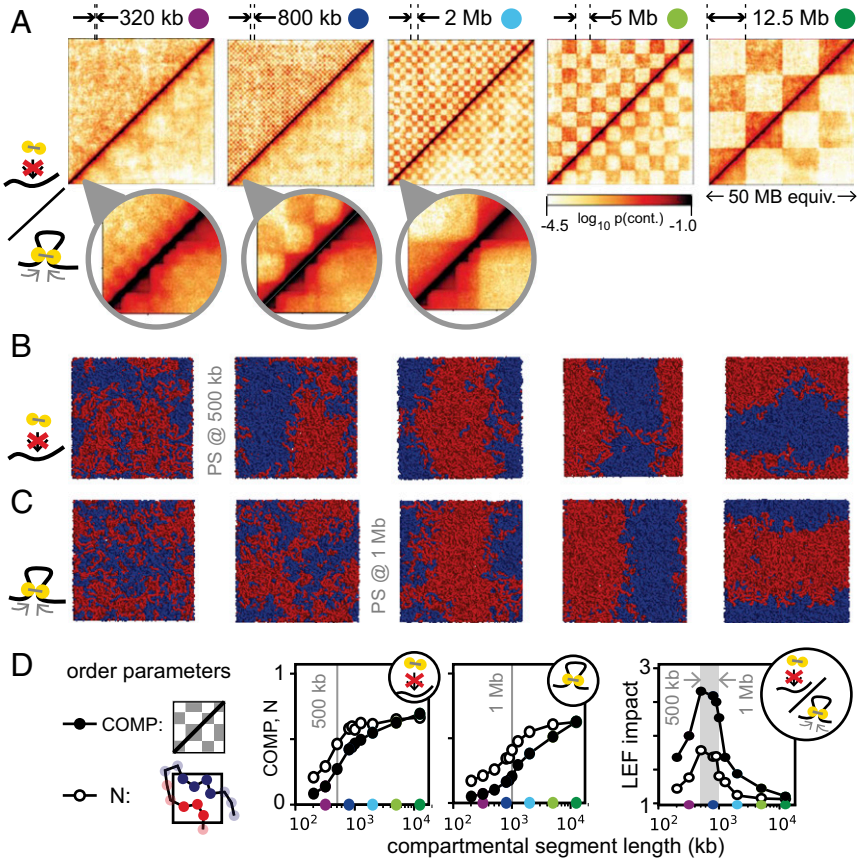

Fig. 3. Impact of loop extrusion on compartments of different size. (*A*) Contact frequency maps without/with loop extrusion (upper/lower triangles). The lengths of A/B segments are indicated above the maps. (*B* and *C*) Example conformations of 50-Mb fibers without/with loop extrusion, in periodic boundary conditions (see *SI Appendix*, Fig. S10 for a comparison with spherical confinement). The approximate segment length where phase separation (PS) occurs is indicated in gray. (*D*) The degree of phase separation as a function of segment length is measured from contact frequency maps (COMP) and from spatial configurations (*N*; see text for details). The impact of loop extrusion on compartmentalization (*Right*) is measured by dividing each of the above order parameters in the absence of loop extrusion by their value with loop extrusion. The impact is maximal for segment lengths that exceed the segregation transition but not the mixing length, which is of the order of several LEF processivities (~1 Mb).

The loss of extrusion barriers while maintaining loop extrusion removes TADs but preserves $P(s)$. Loss of chromatin-associated cohesin in experiments, on the contrary, leads to the reduced compaction as evident by the loss of the hump in the $P(s)$ curve. Simulations with diminished loop extrusion activity reproduced these changes (see above and Fig. 2*A*). Corresponding changes in compartmentalization upon cohesin loss and the lack of such changes upon CTCF removal suggest that it is the loop extrusion activity of cohesin that led to coarsening of compartmentalization in the WT.

Increased Loop Extrusion Activity Suppresses Compartments and Enhances TADs. Finally, we consider how increased processivity and amount of cohesin due to depletion of the cohesin unloading factor WAPL can affect compartmentalization. Hi-C data for WAPL-depleted cells show weaker compartmentalization and a strengthening of large TADs and corner peaks (Fig. 2*C*, *Left*) (12, 14). To determine simulation parameters for WAPL depletion, we note that in experiments the amount of chromatin-associated cohesin in WAPL-depleted cells increases moderately (≈1.5- to 2-fold), while the residence time increased considerably (>5-fold) (12, 14). We thus increased the LEF density 1.5-fold (reducing the average separation from 750 to 500 kb) and the residence time 10-fold, which results in larger processivity (2.5 Mb instead of 250 kb). The average loop size increased only 2.6-fold (from 173 to 449 kb), as expected theoretically (48), indicating that extrusion becomes limited by LEFs bumping into each other. In agreement with experiments, this leads to TADs with more pronounced corner peaks (Fig. 2*C*, *Right*). Corner peaks between nonadjacent TAD boundaries are particularly enhanced. We point out that such secondary corner peaks do not per se imply that extruded loops extend beyond TAD boundaries. In simulations, such secondary peaks can emerge either by LEFs crossing a permeable barrier at the TAD boundary, or from nonadjacent extrusion barriers being brought into spatial proximity when LEFs extrude most of the intervening fiber in each TAD (Fig. 2*C* and *SI Appendix*, Fig. S3). To what extent actual loop extrusion enzymes cross TAD boundaries will be an interesting question for future experiments. The change in the contact probability $P(s)$ in our simulations is also consistent with changes in experimental $P(s)$ curves (Fig. 2*C*, *Lower*), which show an extension of the characteristic hump to larger genomic separations, reflecting larger extruded loops.

Also in agreement with experiments, our simulations of WAPL depletion show reduced compartmentalization (Fig. 2*C*). We attribute this to increased compartment mixing by the increased number of LEFs and increased loop length. Further suppression of compartments in WAPL-depleted cells might be due to formation of axially compressed and stiff "vermicelli" chromosomes (52), which can limit far-*cis* contacts and interactions with the lamina, thus affecting compartmentalization.

The Nonequilibrium Nature of Loop Extrusion Is Central to Compartment Mixing and TAD Strength. We have shown above that compartment mixing by loop extrusion explains the changes of TADs and compartmentalization for all considered experimental perturbations. We thus aim at understanding physical mechanisms behind this mixing effect.

The active process of loop extrusion can bring loci into contact irrespective of their compartmental identity and thereby counteract the phase separation structure from compartmental interaction. We thus asked whether the reduced compartmentalization due to loop extrusion can be simply understood by an effective reduction of the compartmental interaction. To test this, we run simulations without loops, but instead we lowered the B–B attraction until the degree of compartmentalization fell below the value achieved by adding loop extrusion (*SI Appendix*, Fig. S4). We find, however, that Hi-C maps (*SI Appendix*, Fig. S4*A*) and the compartment profile autocorrelation (*SI Appendix*, Fig. S4*E*) behave differently. Indeed, for reduced B–B attraction, we see little evidence of compartment coarsening, that is, loss of shorter compartment regions, as the autocorrelation barely changed. We thus conclude that the impact loop extrusion on compartmentalization cannot be described by a reduced compartmental interaction.

Next, we asked whether the active, nonequilibrium nature of loop extrusion is essential for its interference with compartmentalization. The process of loop extrusion (i.e., loops are born, grow, and then are released when the LEF dissociates) can interfere with compartmentalization in two distinct ways: (*i*) by the mere presence of loops that compact chromatin and connect loci irrespective of their compartmental identity, and (*ii*) by the active nature of loop extrusion that can increase compartment mixing because loci need some time to resegregate after being brought into contact by active loop extrusion.

To examine the relative contributions of these factors, we compare dynamically growing loops and static loops. We choose an ensemble of static loops from simulations with loop extrusion, but now loops remain static while the chromatin fiber is subject to thermal motion (see *SI Appendix* for details). We find that TADs are still visible in the corresponding Hi-C maps (Fig. 4*A*) and TAD averages (Fig. 4*B*), albeit weaker. Surprisingly, the degree of compartmentalization for static loops is almost as strong as when loops are completely absent (Fig. 4*C*). Also, the compartment profile autocorrelation for static loops resembles that without loops (*SI Appendix*, Fig. S5*E*). To generalize the dichotomy of static vs. dynamic loops, we varied the loop extrusion speed while keeping the thermal motion of the fiber constant (Fig. 4 *A*–*C* and *SI Appendix*, Fig. S5). We found that compartmentalization progressively decreases for faster LEFs (Fig. 4*C*). This suggests that the nonequilibrium nature of loop extrusion is central to its role in compartment mixing: After being zipped together by the passage of an LEF, the fiber has less time to resegregate before passage of the next LEF when LEFs dynamics are fast. Furthermore, we found that the speed of extrusion also affects TAD strength: Fast LEFs lead to stronger TADs, while static loops lead to weak TADs (Fig. 4 *A*–*C*; see *SI Appendix* for definition of TAD strength). The impact of LEF speed on TAD strength is particularly apparent when averaging contact maps over many TADs (Fig. 4*B*; see *SI Appendix*, Fig. S5 for TAD size dependence). This, again, reflects the nonequilibrium nature of loop extrusion: TADs are more compact and thus more pronounced in Hi-C data if LEF dynamics are accelerated relative to polymer diffusion dynamics (see *SI Appendix*, Fig. S6 for a cartoon explanation). Taken together, our results suggest that static loops contribute little to the observed compartment mixing and to TAD strength, indicating that the nonequilibrium nature of active loop extrusion is central both to interference with compartmentalization and establishment of pronounced TADs.

It is important to emphasize that when changing LEF speed in simulations we made sure to maintain other macroscopic characteristics such as processivity, loop sizes, and the distribution of genomic LEF positions: We only altered LEF dynamics relative to thermal polymer diffusion (this applies in particular to our static loops, which are found at all positions within TADs and should not be confused with hypothetical loops connecting only TAD borders). The important effect of increasing LEF speed is that the fiber has less time to equilibrate by thermal motion between passages of LEFs and is thereby kept further from thermodynamic equilibrium. Our finding that TAD strength and compartment mixing depend on LEF speed is thus a direct consequence of the nonequilibrium nature loop extrusion.

The nonequilibrium effect of active loop extrusion can be further strengthened by topological effects such as entrapment of the fiber in the dense network of chromatin surrounding it (55, 56). It is well known that the amount of chain passing, which is enabled by topoisomerase II activity in the cell nucleus, has a

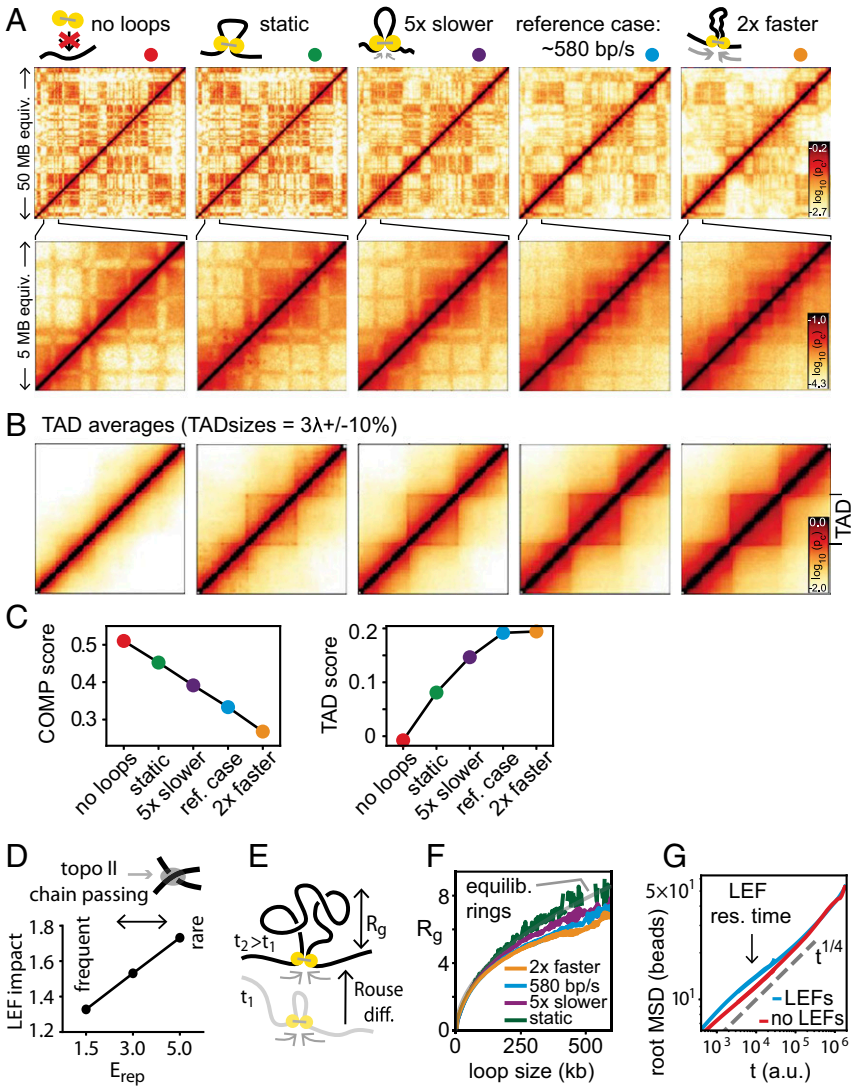

Fig. 4. The nonequilibrium nature of loop extrusion. (*A–C*) Effects of the speed of loop extrusion relative to thermal polymer dynamics. (*A*) Contact frequency maps. (*B*) Averages of TADs of sizes 675–825 kb rescaled to fixed size (see *SI Appendix*, Fig. S5 for other TAD sizes). (*C*) Strength of compartmentalization and of TADs score as a function of LEF speed: Compartmentalization decreases while TAD strength increases from no loops over static loops to extruding loops of increasing speed (the polymer dynamics due to thermal motion are kept constant). (*D*) Importance of chain passing: The impact of loop extrusion on compartmentalization, measured by the ratio of compartmentalization strength without/with loop extrusion, increases for reduced topoisomerase II activity, that is, reduced chain passing (implemented by increasing E_{rep}, the repulsive part of the monomer interaction potential; *SI Appendix*, Fig. S1). (*E*) Length scales relevant for equilibration of a loop: radius of gyration of an extruded loop R_g and diffusional displacement during loop growth. (*F*) R_g follows equilibrium theory (gray) for static loops, while with increasing LEF speed loops are more compact. R_g is measured in units of one monomer diameter of ≈50 nm. (*G*) The root-mean-square displacement of chromatin with/without loop extrusion differs on the LEF residence timescale, but not globally, indicating that loop extrusion cannot be described as an elevated effective temperature.

great influence on relaxation times of polymer systems (39, 40). We thus alter the stringency of such topological constraints by changing the energy barrier for chain passing, that is, the repulsive core of the monomer interaction potential E_{rep}. We find that more stringent topological constraints reduce compartmentalization (*SI Appendix*, Fig. S7) and that the impact of loop extrusion on compartmentalization increases (Fig. 4*D*). Thus, our findings suggest that loop extrusion keeps chromatin far from equilibrium, with topological constraints reinforcing this effect.

The nonequilibrium nature of loop extrusion not only leads to compartmental mixing but also directly affects other characteristics of the chromatin fiber that can potentially be addressed experimentally. In particular, we consider the 3D size of an extruded loop, as measured by its radius of gyration R_g (Fig. 4*E* and *SI Appendix*). We find that actively extruded loops are more compact than static loops and that the compaction increases with LEF speed (Fig. 4*F*; see *SI Appendix* for details). This is expected, because loci that are brought into proximity by loop extrusion need time to move apart by thermal diffusion (Rouse diffusion, Fig. 4*E*). Finally, we ask how active loop extrusion is reflected in the overall dynamics of the chromatin fiber by measuring its mean square displacement (MSD). Specifically, we asked whether loop extrusion could be understood as an increased effective temperature, a conceivable consequence of the energy input from molecular motors. We find, however, that the MSD is elevated only on the timescale of loop extrusion without affecting the displacement on longer times (Fig. 4*G*). This is inconsistent with an elevated effective temperature, which would increase MSDs uniformly.

In conclusion, we found that neither (*i*) elevated effective temperature, nor (*ii*) static or very slow loops, nor (*iii*) reduced

compartmental interaction can reproduce the effects of loop extrusion, which underlines that it is a true nonequilibrium effect that can be thought of as active mixing of the polymer system. Experimental ramifications of these findings are discussed below.

Changes in TADs and Compartmentalization Can Reveal the Underlying Mechanisms. To consolidate our results, we consider how the strengths of TADs and compartments are connected to each other, and how they can be altered by biological perturbations at the molecular level. To this end, we measure how the strengths of TADs and compartments change as we vary (*i*) the characteristics of the loop extrusion machinery, namely LEF processivity (or residence time, *SI Appendix*, Fig. S9), LEF density (*SI Appendix*, Fig. S2), and LEF speed (*SI Appendix*, Fig. S5); (*ii*) topological properties, that is, the frequency of chain passing (*SI Appendix*, Fig. S7); (*iii*) the permeability of extrusion barriers (*SI Appendix*, Fig. S3); (*iv*) the strength of epigenetically encoded compartmental interaction (*SI Appendix*, Fig. S4); and (*v*) nuclear volume (*SI Appendix*, Fig. S8). In each case, we start from our "WT" parameters and sweep a single parameter to examine how compartmentalization and TAD strengths change. Strikingly, we find that different perturbations lead to different changes in the compartmentalization-vs.-TAD strength diagram.

We find (Fig. 5) that alterations of the loop extrusion process, namely of the residence time of LEFs, their linear density, and the speed of extrusion, result in simultaneous changes in TADs and compartmentalization: Reduced loop extrusion activity leads to weaker TADs and stronger (more segregated) compartments. Interestingly, changes in topological properties, simulating activation or inhibition of topoisomerase II (i.e., allowing more or fewer chain passings), show a similar trend. Alteration of the extrusion barrier permeability, however, shows a different pattern: It strongly affects TADs but leaves compartmentalization almost unaffected (as loop extrusion is preserved; see above). Strikingly, when nuclear volume or the compartmental interaction (i.e., B–B attraction) is changed, we observe a third type of behavior: changes in compartmentalization but not in the strength of TADs.

Our joint analysis of variations in TADs and compartmentalization provides an approach to interpreting existing and future experimental data, suggesting that coordinated changes in TADs and compartments reflect changes in the loop extruding machinery of cohesin or topoisomerase II activity; changes in TADs that leave compartments unaffected most likely come from altered extrusion barrier permeability [determined by binding of boundary proteins such as CTCF, and potentially YY1 (57) and Znf143, either globally or at specific loci]; and changes in compartments that do not affect TADs reflect changes in nuclear volume or in the epigenetic landscape of histone modifications or the molecules that mediate their interactions.

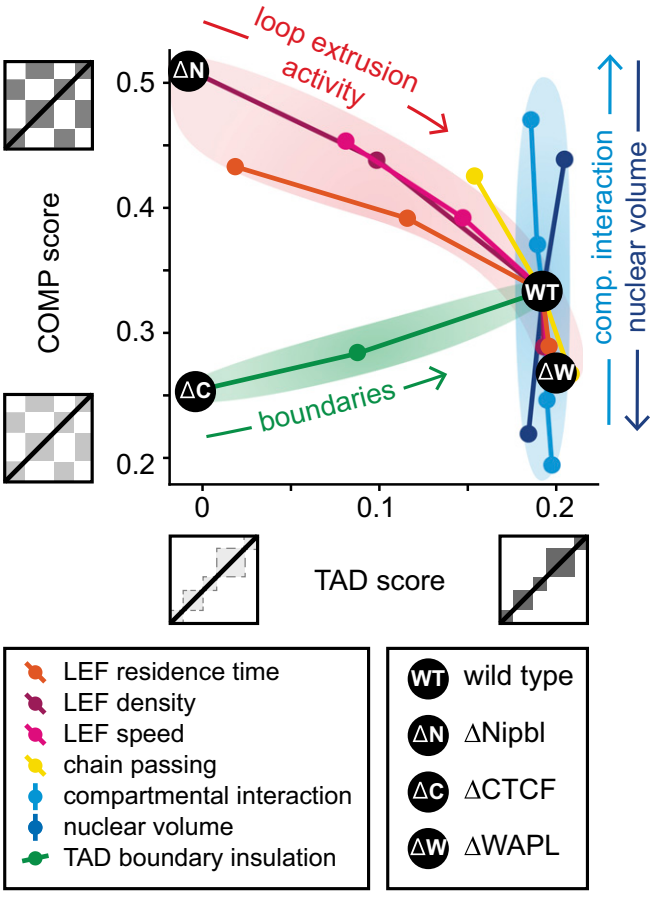

Fig. 5. Effects of different mechanisms on TAD and compartment strength. Three main classes of responses to perturbations are identified: A trade-off between compartmentalization and TADs is observed for parameter changes related to cohesin dynamics and for the frequency of chain passing (topoisomerase II activity). Compartmental interaction and nuclear volume mainly affect compartmentalization. The permeability of extrusion barriers mainly affects TADs. The black dots indicate our simulations of WT interphase cells and removal of cohesin (by Nipbl deletion), of CTCF, and of WAPL.

Discussion

We have elucidated a key step toward a complete model of interphase chromatin: the interplay of loop extrusion and compartmental segregation, two mechanisms that shape major features of chromosome organization in vertebrates. Motivated by recent experiments that point toward such an interplay (12, 37), we used polymer models of chromosomes to investigate whether simultaneous action of loop extrusion and compartmental segregation can quantitatively reproduce experimental findings. We found that this is indeed the case for all three perturbations, namely removal of chromatin-associated cohesin by Nipbl removal, removal of the TAD boundary protein CTCF, and removal of the cohesin unloader WAPL. The key insight is that loop extrusion counteracts compartmental segregation. This argues against a hierarchical organization that claims that TADs are building blocks of compartments and replaces it with a more complex picture where the active loop extrusion partially overrides innate compartmentalization preferences.

Specifically, we found that (*i*) removal of the cohesin loader Nipbl reveals the intrinsic compartment structure because segregation is no longer suppressed by loop extrusion. (*ii*) Removal of the boundary element CTCF removes TADs because without extrusion barriers loops are not confined to specific domains, but they continue to locally compact chromatin and to counteract compartmental segregation. (*iii*) Removal of the cohesin unloading factor WAPL increases cohesin residence time on DNA and thereby increases both the number of loops as well as loop length, which at the same time strengthens TADs and weakens compartmentalization due to enhanced compartment mixing.

Our mechanistic model relies on simplifying assumptions that we now address. First, the microscopic biophysical mechanisms that drive compartmental segregation remain unknown. Here, we assumed a phase separation process, in line with experimental indications for heterochromatin formation (46, 47), which we induced by a specific short-range attraction between chromatin loci of type B. This constitutes a minimal model for compartmental segregation. Other interaction potentials or even different mechanisms of segregation could be present as well. For example, segregation based on differences in activity instead of contact interaction is a plausible scenario (58–60).

Within the phase separation scenario that we presented here and in ref. 54, three aspects are important to point out: First, as demonstrated in Fig. 3, phase separation requires compartmental segments above a critical length, and short ones may fail to segregate. Second, the connectedness of euchromatin and heterochromatin segments into a single fiber restricts the formation of macroscopic phases observed in bona fide phase separation. Rather, a multitude of patterns depending of the segment sizes and mixing ratios can emerge, referred to as microphase separation, a phenomenon that is typical for block copolymers (39, 40). Last, for a more complete picture, one may want to model the role of interactions between heterochromatin and the nuclear lamina. Our focus on B–B interactions is motivated by the observation that rod cells lacking naturally (54) or artificially (61) lamin and/or B receptor show global reorganization of chromatin with euchromatin moving to the center, but nevertheless exhibit similar compartmentalization as rod cells in their natural state. We point out that global reorganizations can be facilitated by phase separation: When parts of a certain type of chromatin are tethered to the lamina or other nuclear bodies, the rest of the same type may follow.

As another simplifying assumption, we studied the interplay of loop extrusion and compartmental segregation in steady state, that is, simulations were run long enough to forget the initial configurations before quantities of interest were measured. We thereby established a somewhat idealized reference case. A more realistic picture would start from mitotic chromosomes (55), where neither compartments nor TADs are observed (20, 62), which we leave for future investigations.

Furthermore, the microscopic details behind loop extrusion remain enigmatic. In particular, processive motion (28) and real-time, one-sided loop extrusion (29) have been demonstrated in in vitro only for condensins, while corresponding evidence is still missing for cohesins, which are relevant in higher eukaryotes in interphase. Furthermore, experiments are at odds with a simple picture where the sole function of the Nipbl complex (also termed SCC2/SCC4) is to facilitate cohesin loading while WAPL determines its residence time on chromatin, and rather suggest that SCC4 also regulates the processivity and/or the residence time of cohesin on DNA (12), that WAPL/PDS5 assists in loading and unloading (63), and that transcription plays a major role in positioning cohesins (64). Consequently, several parameters in our mechanistic model of loop extrusion are known with limited accuracy. Those include the number of DNA-bound loop extruding factors, their processivity, their speed, details about the extrusion process (e.g., one-sided vs. two-sided), and interaction with other proteins like CTCF, Nipbl, WAPL, and PDS5 (14). In light of such uncertainties, we use simulations to establish consistency of our mechanistic model with experimental observations (see ref. 65 for a review).

Surprisingly, our relatively simple and general mechanistic model was able to achieve consistency with experiments reproducing a number of features, such as TADs, compartmentalization, and the contact probability $P(s)$ curves, for a diverse set of unrelated experimental perturbations. In the future, an iterative process of increasingly specific experiments and more constrained simulations will show how far the loop extrusion and compartment segregation model can go in quantitatively explaining chromatin organization.

We finally discuss experimental ramifications and potential tests of our model. While our study was motivated by specific alterations of the loop extrusion machinery (namely, cohesin abundance, processivity, and barrier permeability), our results go beyond explaining these experiments and make specific predictions. In particular, experimental alteration of the speed of LEFs would reveal to what extent WT TADs are nonequilibrium structures and thereby potentially rule out permanent chromatin loops as a possible explanation of TADs. With respect to the interplay of TADs and compartments, experiments where the speed of LEFs or topoisomerase II activity is altered are expected to see a trade-off between TAD strength and compartmentalization. Conversely, perturbations altering the nuclear volume or the compartmental interaction, for example, by changing the epigenetic landscape or mediators of compartment interactions, possibly HP1 (46, 47), are expected to affect compartmentalization, while leaving TADs unaffected. Furthermore, we showed that when faced with an experimental phenotype for which the underlying microscopic alteration is not known, the joint variation of TADs and compartmentalization can help to unravel it: Variations in TAD strength alone indicate that only TAD boundaries are affected, variations in compartmentalization alone indicate that the compartmental interaction is changed, while a trade-off between TAD strength and compartmentalization stems from changed cohesin dynamics or topoisomerase II activity. As an example, a recent comparison of maternal and paternal pronuclei demonstrated similar TAD strength, but considerably weaker compartmentalization in maternal zygotes; our results here suggest that this is due to differences in the epigenetic landscape, and possibly a lack of heterochromatin in those pronuclei (10). Finally, we found that characteristics of the 3D folding of chromatin bear information about specific aspects of loop extrusion: Loops are more compact in 3D space when extrusion is fast, consistent with the observation that changing extrusion speed can disentangle contact frequency from average spatial distances (66). As high-resolution (7, 67, 68) and live-cell (69–71) imaging of chromatin is making dramatic progress, such questions may be addressed in the near future.

In conclusion, our work shows that the interplay of active loop extrusion and compartmental segregation shapes chromosome organization in interphase. More broadly, we hope that the principle that active processes can oppose equilibrium energetics, can serve as a paradigm for future biophysical research.

Methods

Our study relies on coarse-grained molecular-dynamics simulations of chromatin subject to loop extrusion and compartment segregation. Simulations were performed based on OpenMM (72, 73). In brief, our approach is to generate a large number of polymer conformations from which a simulated Hi-C experiment produces contact frequency maps that are compared with experimental Hi-C data. We typically simulated a 20,000 monomer chain, with one monomer corresponding to 2.5 kb. The TAD structure was defined by random positioning of extrusion barriers along the polymer. The average TAD size was 375 kb (150 monomers). Compartments were also placed randomly and not correlated with TADs. We used a randomly generated TAD and compartment structure because, first, there is no uniquely agreed-upon method for calling them from experimental data; second, because we wanted to compare one unified set of simulations to three different sets of experimental data; and, finally, because our results on aggregated quantities, like the degree of compartmentalization, compartment profile autocorrelations, and contact probability scaling, can be equally well made with random TADs and compartments. LEFs are implemented as bonds between not necessarily adjacent monomers. When an LEF takes a step from, say, monomers (i, j) to monomers $(i - 1, j + 1)$, the old bond is deleted and is replaced with a new bond. Full details are given in *SI Appendix*.

ACKNOWLEDGMENTS. We gratefully acknowledge funding from National Science Foundation Grant 1504942 (Physics of Chromosomes) and NIH Grant GM114190 (Polymer Models of Mitotic and Interphase Chromosomes) (to L.A.M.), and support of the 4D Nucleome NIH Initiative DK107980 (Center for 3D Structure and Physics of the Genome).

1. Dekker J, Rippe K, Dekker M, Kleckner N (2002) Capturing chromosome conformation. *Science* 295:1306–1311.
2. Lieberman-Aiden E, et al. (2009) Comprehensive mapping of long-range interactions reveals folding principles of the human genome. *Science* 326:289–293.
3. Imakaev M, et al. (2012) Iterative correction of Hi-C data reveals hallmarks of chromosome organization. *Nat Methods* 9:999–1003.
4. Bonev B, Cavalli G (2016) Organization and function of the 3D genome. *Nat Rev Genet* 17:661–678.

5. Osborne CS, et al. (2004) Active genes dynamically colocalize to shared sites of ongoing transcription. *Nat Genet* 36:1065–1071.
6. Simonis M, et al. (2006) Nuclear organization of active and inactive chromatin domains uncovered by chromosome conformation capture-on-chip (4C). *Nat Genet* 38: 1348–1354.
7. Wang S, et al. (2016) Spatial organization of chromatin domains and compartments in single chromosomes. *Science* 353:598–602.
8. Nora EP, et al. (2012) Spatial partitioning of the regulatory landscape of the X-inactivation centre. *Nature* 485:381–385.
9. Dixon JR, et al. (2012) Topological domains in mammalian genomes identified by analysis of chromatin interactions. *Nature* 485:376–380.
10. Gassler J, et al. (2017) A mechanism of cohesin-dependent loop extrusion organizes zygotic genome architecture. *EMBO J* 36:3600–3618.
11. Schwarzer W, et al. (2017) Two independent modes of chromatin organization revealed by cohesin removal. *Nature* 551:51–56.
12. Haarhuis JHI, et al. (2017) The cohesin release factor WAPL restricts chromatin loop extension. *Cell* 169:693–707.e14.
13. Rao SSP, et al. (2017) Cohesin loss eliminates all loop domains. *Cell* 171:305–320.e24.
14. Wutz G, et al. (2017) Topologically associating domains and chromatin loops depend on cohesin and are regulated by CTCF, WAPL, and PDS5 proteins. *EMBO J* 36: 3573–3599.
15. Sanborn AL, et al. (2015) Chromatin extrusion explains key features of loop and domain formation in wild-type and engineered genomes. *Proc Natl Acad Sci USA* 112: E6456–E6465.
16. Fudenberg G, et al. (2016) Formation of chromosomal domains by loop extrusion. *Cell Rep* 15:2038–2049.
17. Riggs AD (1990) DNA methylation and late replication probably aid cell memory, and type I DNA reeling could aid chromosome folding and enhancer function. *Philos Trans R Soc Lond B Biol Sci* 326:285–297.
18. Nasmyth K (2001) Disseminating the genome: Joining, resolving, and separating sister chromatids during mitosis and meiosis. *Annu Rev Genet* 35:673–745.
19. Alipour E, Marko JF (2012) Self-organization of domain structures by DNA-loop-extruding enzymes. *Nucleic Acids Res* 40:11202–11212.
20. Naumova N, et al. (2013) Organization of the mitotic chromosome. *Science* 342: 948–953.
21. Hirano T (2016) Condensin-based chromosome organization from bacteria to vertebrates. *Cell* 164:847–857.
22. Uhlmann F (2016) SMC complexes: From DNA to chromosomes. *Nat Rev Mol Cell Biol* 17:399–412.
23. Sofueva S, et al. (2013) Cohesin-mediated interactions organize chromosomal domain architecture. *EMBO J* 32:3119–3129.
24. Haering CH, Farcas A-M, Arumugam P, Metson J, Nasmyth K (2008) The cohesin ring concatenates sister DNA molecules. *Nature* 454:297–301.
25. Stigler J, Çamdere GÖ, Koshland DE, Greene EC (2016) Single-molecule imaging reveals a collapsed conformational state for DNA-bound cohesin. *Cell Rep* 15:988–998.
26. Davidson IF, et al. (2016) Rapid movement and transcriptional re-localization of human cohesin on DNA. *EMBO J* 35:2671–2685.
27. Rao SSP, et al. (2014) A 3D map of the human genome at kilobase resolution reveals principles of chromatin looping. *Cell* 159:1665–1680.
28. Terakawa T, et al. (2017) The condensin complex is a mechanochemical motor that translocates along DNA. *Science* 358:672–676.
29. Ganji M, et al. (2018) Real-time imaging of DNA loop extrusion by condensin. *Science* 360:102–105.
30. Wang X, Brandão HB, Le TBK, Laub MT, Rudner DZ (2017) *Bacillus subtilis* SMC complexes juxtapose chromosome arms as they travel from origin to terminus. *Science* 355:524–527.
31. Ciosk R, et al. (2000) Cohesin's binding to chromosomes depends on a separate complex consisting of Scc2 and Scc4 proteins. *Mol Cell* 5:243–254.
32. Gandhi R, Gillespie PJ, Hirano T (2006) Human Wapl is a cohesin-binding protein that promotes sister-chromatid resolution in mitotic prophase. *Curr Biol* 16:2406–2417.
33. Kueng S, et al. (2006) Wapl controls the dynamic association of cohesin with chromatin. *Cell* 127:955–967.
34. Guo Y, et al. (2015) CRISPR inversion of CTCF sites alters genome topology and enhancer/promoter function. *Cell* 162:900–910.
35. de Wit E, et al. (2015) CTCF binding polarity determines chromatin looping. *Mol Cell* 60:676–684.
36. Narendra V, et al. (2015) CTCF establishes discrete functional chromatin domains at the Hox clusters during differentiation. *Science* 347:1017–1021.
37. Nora EP, et al. (2017) Targeted degradation of CTCF decouples local insulation of chromosome domains from genomic compartmentalization. *Cell* 169:930–944.e22.
38. Misteli T (2007) Beyond the sequence: Cellular organization of genome function. *Cell* 128:787–800.
39. Grosberg AY (1994) *Statistical Physics of Macromolecules* (AIP Press, New York).
40. Rubinstein M, Colby R (2003) *Polymer Physics* (Oxford Univ Press, Oxford).
41. Jost D, Carrivain P, Cavalli G, Vaillant C (2014) Modeling epigenome folding: Formation and dynamics of topologically associated chromatin domains. *Nucleic Acids Res* 42:9553–9561.
42. Di Pierro M, Zhang B, Aiden EL, Wolynes PG, Onuchic JN (2016) Transferable model for chromosome architecture. *Proc Natl Acad Sci USA* 113:12168–12173.
43. Jost D, Vaillant C, Meister P (2017) Coupling 1D modifications and 3D nuclear organization: Data, models and function. *Curr Opin Cell Biol* 44:20–27.
44. Filion GJ, et al. (2010) Systematic protein location mapping reveals five principal chromatin types in *Drosophila* cells. *Cell* 143:212–224.
45. Collepardo-Guevara R, et al. (2015) Chromatin unfolding by epigenetic modifications explained by dramatic impairment of internucleosome interactions: A multiscale computational study. *J Am Chem Soc* 137:10205–10215.
46. Strom AR, et al. (2017) Phase separation drives heterochromatin domain formation. *Nature* 547:241–245.
47. Larson AG, et al. (2017) Liquid droplet formation by HP1α suggests a role for phase separation in heterochromatin. *Nature* 547:236–240.
48. Goloborodko A, Marko JF, Mirny LA (2016) Chromosome compaction by active loop extrusion. *Biophys J* 110:2162–2168.
49. Nakahashi H, et al. (2013) A genome-wide map of CTCF multivalency redefines the CTCF code. *Cell Rep* 3:1678–1689.
50. Hansen AS, Pustova I, Cattoglio C, Tjian R, Darzacq X (2017) CTCF and cohesin regulate chromatin loop stability with distinct dynamics. *eLife* 6:e25776.
51. Gerlich D, Koch B, Dupeux F, Peters J-M, Ellenberg J (2006) Live-cell imaging reveals a stable cohesin-chromatin interaction after but not before DNA replication. *Curr Biol* 16:1571–1578.
52. Tedeschi A, et al. (2013) Wapl is an essential regulator of chromatin structure and chromosome segregation. *Nature* 501:564–568.
53. Rhodes J, et al. (2017) Cohesin can remain associated with chromosomes during DNA replication. *Cell Rep* 20: 2749–2755.
54. Falk M, et al. (January 9, 2018) Heterochromatin drives organization of conventional and inverted nuclei. bioRxiv:10.1101/244038.
55. Rosa A, Everaers R (2008) Structure and dynamics of interphase chromosomes. *PLoS Comput Biol* 4:e1000153.
56. Brackley CA, Allan J, Keszenman-Pereyra D, Marenduzzo D (2015) Topological constraints strongly affect chromatin reconstitution in silico. *Nucleic Acids Res* 43:63–73.
57. Weintraub AS, et al. (2017) YY1 is a structural regulator of enhancer-promoter loops. *Cell* 171:1573–1588.e28.
58. Ganai N, Sengupta S, Menon GI (2014) Chromosome positioning from activity-based segregation. *Nucleic Acids Res* 42:4145–4159.
59. Grosberg AY, Joanny JF (2015) Nonequilibrium statistical mechanics of mixtures of particles in contact with different thermostats. *Phys Rev E Stat Nonlin Soft Matter Phys* 92:032118.
60. Smrek J, Kremer K (2017) Small activity differences drive phase separation in active-passive polymer mixtures. *Phys Rev Lett* 118:098002.
61. Solovei I, et al. (2013) LBR and lamin A/C sequentially tether peripheral heterochromatin and inversely regulate differentiation. *Cell* 152:584–598.
62. Gibcus JH, et al. (2018) A pathway for mitotic chromosome formation. *Science* 359: eaao6135.
63. Murayama Y, Uhlmann F (2015) DNA entry into and exit out of the cohesin ring by an interlocking gate mechanism. *Cell* 163:1628–1640.
64. Busslinger GA, et al. (2017) Cohesin is positioned in mammalian genomes by transcription, CTCF and Wapl. *Nature* 544:503–507.
65. Fudenberg G, Abdennur N, Imakaev M, Goloborodko A, Mirny LA (2018) Emerging evidence of chromosome folding by loop extrusion. *Cold Spring Harb Symp Quant Biol* 2018:034710.
66. Fudenberg G, Imakaev M (2017) FISH-ing for captured contacts: Towards reconciling FISH and 3C. *Nat Methods* 14:673–678.
67. Boettiger AN, et al. (2016) Super-resolution imaging reveals distinct chromatin folding for different epigenetic states. *Nature* 529:418–422.
68. Ou HD, et al. (2017) ChromEMT: Visualizing 3D chromatin structure and compaction in interphase and mitotic cells. *Science* 357:eaag0025.
69. Gu B, et al. (2018) Transcription-coupled changes in nuclear mobility of mammalian *cis*-regulatory elements. *Science* 359:1050–1055.
70. Lucas JS, Zhang Y, Dudko OK, Murre C (2014) 3D trajectories adopted by coding and regulatory DNA elements: First-passage times for genomic interactions. *Cell* 158: 339–352.
71. Bronshtein I, et al. (2015) Loss of lamin A function increases chromatin dynamics in the nuclear interior. *Nat Commun* 6:8044.
72. Eastman P, Pande VS (2015) OpenMM: A hardware independent framework for molecular simulations. *Comput Sci Eng* 12:34–39.
73. Eastman P, et al. (2013) OpenMM 4: A reusable, extensible, hardware independent library for high performance molecular simulation. *J Chem Theory Comput* 9:461–469.